Local Binary Pattern based features for Prostate Cancer Detection

KAI Harsha[1#], MB Rathnayaka[2,3] and DK Hewadikaram[1]

[1]*General Sir John Kotelawala Defence University, Ratmalana, Sri Lanka*
[2]*University of Colombo, Colombo*
[3]*Utsouthwestern, University of Texas, Texas, USA*

#harsha99indu@gmail.com

Abstract:*Prostate cancer is one of the most common cancers in males and one of the significant causes of cancer mortality. Most prostate malignancies are presently diagnosed based on an increased PSA level, despite this biomarker having only limited accuracy. Prostate cancer differs from most other cancers because it is frequently multifocal and does not appear as a single spherical mass. The illness progresses at different rates, and it is frequently asymptomatic until it has gone to late stages Multi-parametric MRI (mpMRI) has advanced dramatically in the last 20 years, as has the treatment of localised prostate cancer. As a result, this research aims to develop an algorithm to identify features based on the Local Binary Pattern (LBP) based histogram and Grey Level Run Length Matrix (GLRLM) characteristics of mpMRI images, to improve detection rate and accuracy of prostate cancer diagnosis. Local binary patterns are texture descriptors that have been effectively employed as image descriptors in various applications. Images were gathered from a public image database to complete this work. The operator is applied to the selected region of interest (ROI) to generate the LBP image. Texture pattern probability was summarised into a histogram, and second-order statistics were obtained using the GLRLM operator. The statistical significance of the eleven characteristics was determined using an independent two-sample t-test using four features from the histogram and seven features from the GLRLM operator. The suggested approach yielded three favourable outcomes in the research, which can be utilised to identify malignant tumours from benign tumours. The positive results include the first-order statistics standard deviation and kurtosis and the second-order statistic Run Length Non-uniformity (RLN).*

Keywords*:Prostate cancer diagnosis, LBP, GLRLM*

1. Introduction

Prostate cancer is the second most common cancer among men, and men with prostate cancer face death at a higher rate than their estimated frequency, as shown in Figure 1. Because prostate cancer is typically multifocal and does not show as a single spherical mass, it is different from most other tumours. The disease advances at varying speeds, and it is typically asymptomatic until it is advanced. According to the Global Cancer Observatory, the incidence and mortality rate of prostate cancer is expected to drastically increase (see Figure 2). Prostate cancer usually has no symptoms in its early stages, but it may be detected by screening, even if it is latent in the body. Physicians have an interesting but difficult task in identifying prostate cancer accurately. In today's medical world, there is a clear link between high prostate-specific-antigen (PSA) findings and prostate cancer diagnosis. Despite its low sensitivity and specificity for identifying prostate cancer, the PSA test remains one of the best conventional indicators for early identification of prostate cancer (Etzioni *et al.*, 2002; Catalona and Loeb, 2005; Mitchell *et al.*, 2005; Schröder and Roobol, 2009).

Current methods have the unintended consequence of over-diagnosing low-risk illnesses while under-diagnosing high-risk

cancers. In those with high PSA levels, histological confirmation is required, which is usually obtained by random transrectal ultrasonography (TRUS) guided prostate biopsy. This approach, on the other hand, provides false-negative outcomes. As a result of these false results, there is a growing understanding of the potential benefits of employing imaging tools to guide biopsy, allowing for better diagnosis of larger tumours that are more likely to be clinically important.

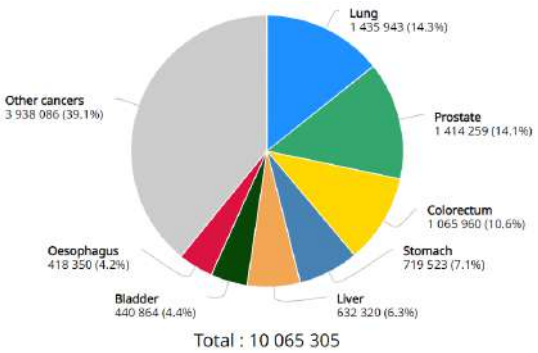

Figure 1. Estimated number of new cases in 2020, worldwide, males, in all ages

Source: GLOBOCAN 2020

A. Multi-parametric Magnetic Resonance Imaging (mpMRI)

The spectrum of available imaging modalities is always growing in response to changes in treatment choices, scientific developments, and technology advancements. One of the earliest imaging modalities to be employed was computed tomography (CT). CT has been replaced by alternative imaging methods such as endorectal, transrectal, ultrasonography for diagnosis and localised staging, and magnetic resonance imaging (MRI) at various institutions since it cannot identify intrinsic prostate cancer.

Among all imaging modalities, mpMRI has emerged as the most efficient and well-established approach for identifying and staging cancers inside the prostate gland (Hricak *et al.*, 2007; Fuchsjager *et al.*, 2008; Seitz *et al.*, 2009; Dinh *et al.*, 2016). mpMRI paired with image-guided biopsy has better-assessed parameters such as the size, location, and staging of distinct lesions inside the prostate than the blood PSA screening test. A mpMRI imaging combines anatomical T2-weighted images with other imaging techniques such as diffusion-weighted (DW) imaging, dynamic contrast-enhanced imaging (DCE), and magnetic resonance spectroscopic imaging (MRSI). T2 weighted MRI imaging aid in the rapid identification of different portions of the prostate, such as the peripheral zone, transition zone, and other structures such as the prostatic capsule, prostatic urethra, and seminal vesicles. Because of their superior resolution, T2 weighted images are also better at identifying the anatomic interactions of the tumour with crucial structures such as the prostatic capsule and neurovascular bundles (Weinreb *et al.*, 2009; Turkbey *et al.*, 2016).

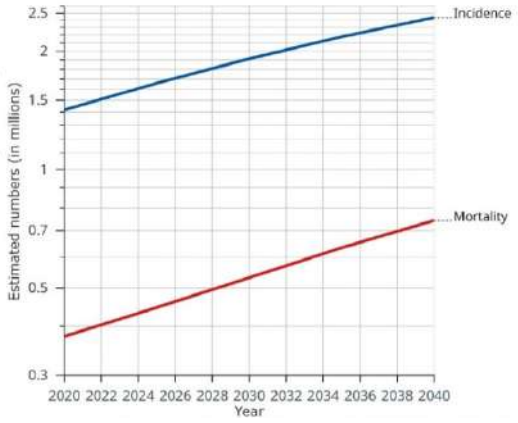

Figure 2. Estimated numbers from 2020 to 2040, age (0-85+)

Source: CANCER TOMORROW | IARC

B. Local Binary Pattern (LBP)

Texture analysis is critical in the field of pattern recognition and classification (Haralick, Dinstein and Shanmugam, 1973; Feng *et al.*, 2015). Initially, classification methods focused mostly on textural image statistical data. The local binary pattern (LBP) was established by Ojala et al. as a texture descriptor for describing 2D textures in grey images (Ojala, Pietikäinen and Harwood, 1996; Ojala *et al.*, 2001). Due to its ease of implementation, quick calculation, and high

efficiency, LBP has already been extensively researched and used in a variety of fields. The importance of using the word "Local" is that the LBP value is continuously computed by examining the pixel characteristic of its surrounding called the neighbourhood. It is explained in the following content how this property can be expressed solely using the numbers "0" and "1," resulting in a 0-1 pattern, which is why the name "Binary Pattern" is used. The centre pixel of the image is obtained by comparing the pixel value to its neighbours. By thresholding each image pixel in the neighbourhood with the pixel value of the centre pixel, a binary value is obtained for each image pixel. A binary pattern may be made out of this binary code by reading the values clockwise or anticlockwise. This process is shown in Figure 3. It is important to remember to maintain the exact starting pixel location and the direction throughout the calculation. Each binary pattern is then converted into a decimal value.

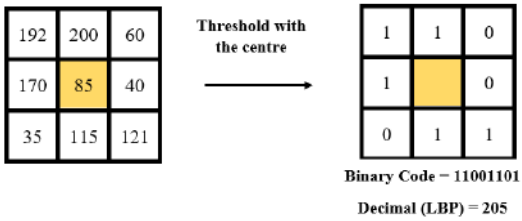

Figure 3. Basic LBP Operator

The LBP code generated is used for classification or segmentation features. As a result, a histogram based on the frequency of binary patterns is constructed. The histogram developed depicts the distribution of local micropatterns such as edges, spots, and flat areas throughout the whole image. Furthermore, while expressing an image, it is critical to keep the spatial information of the pixels in mind.

B. Gray Level Run Length Matrix (GLRLM)

The grey-level run-length matrix (GLRLM) is a matrix that may be used to create texture characteristics for texture analysis of a given ROI. The texture is characterised as grey intensity pixels stretching out from the reference pixels in a specific direction. A grey level run collects pixels with the same grey level score scattered over the ROI in a particular sequence collinearly. The GLRLM is a two-dimensional matrix with each element representing the number of elements j in the direction and the intensity I. Horizontal (0°), anti-diagonal (45°), vertical (90°), and diagonal (135°) are the four primary orientations that are usually considered in an application (see Figure 4).

Galloway initially proposed the run-length method for statistical texture analysis in 1975 (Galloway, 1975). Since then, various applications have been developed based on features created from this technique, including content-based image retrieval, image segmentation, object classification, and many others. Galloway presented five features for classifying the identical set of terrain samples investigated by Haralick (Haralick, Dinstein and Shanmugam, 1973), and the results were auspicious. Long Runs Emphasis (LRE), Short Runs Emphasis (SRE), Gray Level Non-uniformity (GLN), Run Length Non-uniformity (RLN), and Run Percentage (RP) are the features. Chu et al. developed two additional features that employ the grey level distribution of runs instead and are proven to be highly helpful in classification after observing the symmetrical roles played by grey levels and run-length (Chu, Sehgal and Greenleaf, 1990). These two features are said to be analogical to LRE and SRE. In this research, these seven features were extracted from the LBP image of the selected ROI, expecting better classification results. Table 1 lists the features and their computation.

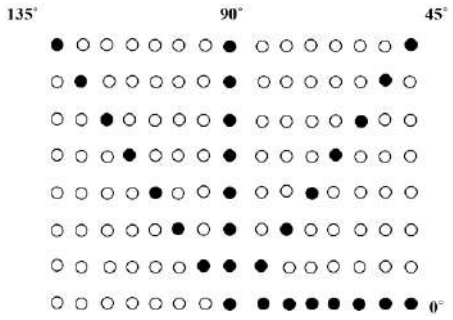

Figure 4. Four main directions of GLRLM computation

C. *The Cancer Imaging Archive (TCIA)*

TCIA is a public-access service that de-identifies and makes a large collection of cancer-related medical images accessible to the public. The information is organized into "collections," which are collections of images from various patients that are linked by a common disease, imaging modality, or research topic. TCIA's principal radiological imaging file format is DICOM. Images are complemented by supporting data such as patient outcomes, treatment information, genomes, and expert assessments when they are available.

2. Methodology

Image Database: PROSTATEx Image Collection

"PROSTATEX" image collection is a collection of MRI studies performed on the prostate from the past study carried out by Litjens et al (Geert Litjens *et al.*, 2017). The collection contains T2-weighted, DCE, DW and proton density-weighted (PD-W) imaging used in research (K *et al.*, 2013; Litjens *et al.*, 2014; Geert Litjens *et al.*, 2017). Litjens et al. obtained a total of 165 subsequent studies with prostate cancer (187 lesions) and 183 patients without prostate cancer for a total of 348 trials of 347 individuals to test the CAD system outlined in the research. A pathologist assessed the biopsy specimens, and the results were utilised as the actual truth. With a score per modality and a point marker, the radiologist identified regions of suspicion. A biopsy was taken if an area was suspected of being cancerous. According to the PI-RADS recommendations for prostate MRI acquisition, all images were taken without the involvement of an endorectal coil. In the subsequent phases, prostate segmentation is necessary to lower the complexity of the detection problem for the classifiers. The segmentation was done using an atlas-based technique. DICOM encoding is used to deliver the obtained MR images. A single study with numerous DICOM images is created for each subject. The DICOM images are divided into several series, each of which contains several instances. Two separate CSV files were used to present the study findings and DICOM image details, named ProstateX-Findings and ProstateX-Images respectively.

Table 1. GLRLM features

Feature
Short Run Emphasis (SRE) $= \frac{1}{n}\sum_{i,j}\frac{p(i,j)}{j^2}$ …(1)
Long Run Emphasis (LRE) $= \frac{1}{n}\sum_{i,j} j^2\, p(1,j)$…(2)
Grey Level Non-uniformity (GLN) $= \frac{1}{n}\sum_i\left(\sum_j p(i,j)\right)^2$ …(3)
Run Percentage (RP) $= \sum_{i,j}\frac{n}{p(i,j)j}$… (4)
Run Length Non-uniformity (RLN) $= \frac{1}{n}\sum_i(\sum_j p(i,j))^2$…(5)
Low Grey Level Run Emphasis (LGRE) $= \frac{1}{n}\sum_{i,j}\frac{p(i,j)}{i^2}$…(6)
High Grey Level Run Emphasis (HGRE) $= \frac{1}{n}\sum_{i,j} i^2 p(i,j)$…(7)

A. *MRI Image Selection*

The images were categorised into training and test sets. The training set included 204 subjects, and the test set included 140 subjects.

From the ProstateX-Findings.csv file, patients with only a fid value of 1 were selected. This means that the patient has only one lesion. Selected patients were then further categorised into 'True' and 'False' categories using the parameter 'ClinSig' in the ProstateX-Findings.csv file. For each of the classified patients, T2-weighted Turbo Spin Echo images from the transversal plane were selected to further proceed in the study. This categorisation process resulted in 76 False and 33 True patient data. The images have been cropped to facilitate image analysis efforts and lessen the detection process's complexity. It was done with the use of an atlas-based segmentation method. The cropped images were of BMP file format. Figure 5(a) and (b) shows the DICOM images of True and False patients from the transversal plane, while Figure 5(c) and (d) depicts the selected cropped images.

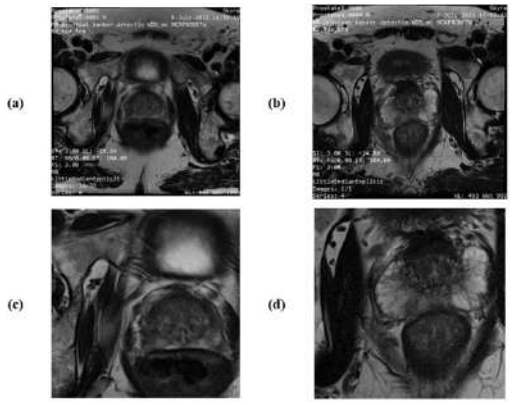

Figure 5. MRI images of the transversal plane. DICOM image of (a) False patient and (b)True patient. Cropped image of (c) False patient and (d) True patient

B. Algorithm Implementation

LBP and GLRLM were proposed to implement the detection algorithm in this research work. To compute the first-order and second-order statistics, the algorithm was built using the MATLAB (2021a) platform with an experimental environment of Windows 11 system and 11th Gen Intel(R) Core (TM) i5 processor 2.40 GHz. The algorithm's phase structure is made up of stages, each of which serves a different purpose. The flow diagram of the algorithms is depicted in Figure 6.

1) Algorithm 1: LBP + Histogram Features: The MRI images were collected from the database POSTATEx Image Collection, and the initial stage in this algorithm is to read them. The second step is to use manual ROI selection to mask out the prostate gland, shown in Figure 7. The function 'roipoly' was used to construct the mask as a binary image for manual ROI selection, setting pixels inside the ROI to 1 and pixels outside the ROI to 0.

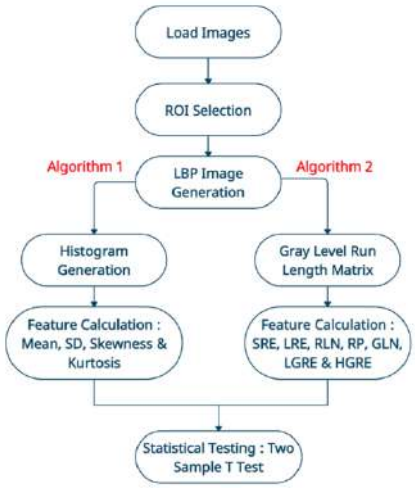

Figure 6. Flow diagram of the proposed algorithms

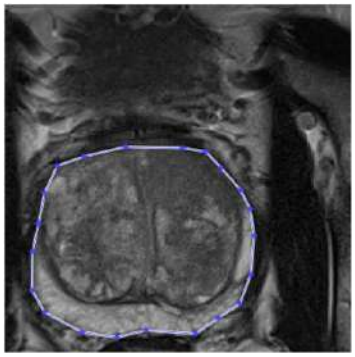

Figure 7. Manual ROI selection of the prostate gland

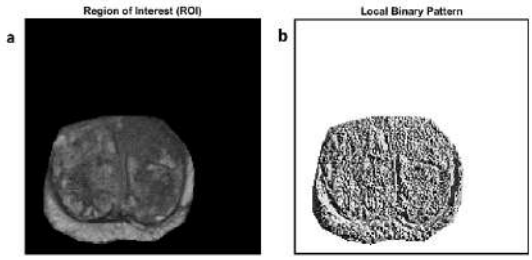

Figure 8. Region of Interest and LBP Image (a) Region of Interest (b) LBP image of the ROI

The next step is to create the LBP image from the chosen ROI, one of the most critical steps. The LBP image was generated using a MATLAB script. Figure 8 shows the ROI selected and the LBP image generated. The histogram of the ROI's LBP image was created after the ROI's LBP image was produced. To accomplish so, the mask's pixels outside the ROI set to 0 were first transformed to NaN (Not a Number) format. The background pixels were then assigned to NaN by scalar multiplying the mask with the LBP image. Then using the functions' unique' and 'accumarray', the grey values and their frequencies of the LBP image was determined. Finally, using the function "bar", the histogram was generated (see Figure 9). determined. Four first-order statistics were calculated using the histogram: mean, skewness, standard deviation, and kurtosis. These features were calculated for both True and False patients, and the results were tabulated.

2) Algorithm 2: LBP + GLRLM Features: Manual ROI selection and LBP image creation utilised the same MATLAB script as for algorithm 1. A user-defined function named 'glrlm' was constructed with reference to a preprogramed script to produce the GLRLM matrix (Elferink, 2021). The newly defined process computed the seven features. The features are SRE, LRE, RLN, RP, GLN, LGRE and HGRE. For statistical testing, the seven features were computed for both True and False patients and tabulated.

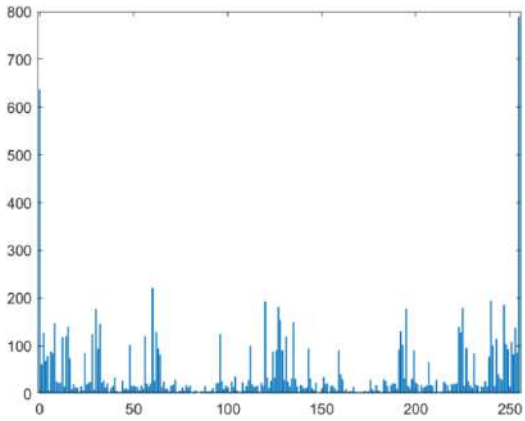

Figure 9. Histogram generated out of an LBP image.

3) Statistical Testing: In the field of research, one is interested in deriving conclusions about a population, yet it is typically impractical or impossible to examine the entire population. Because the goal is frequently to predict the future performance of the proposed system, prototype, or algorithm under similar or different conditions, statistical inference is critical to having rigorous and appropriate tests. The two-sample t-test performed the hypothesis testing of this study. The two-sample independent t-test used in this study confirms if the mean of a normally distributed numerical outcome variable varies between the two separate groups. The variables of the test were the histogram and GLRLM features of True and False patients. The two-sample t-test was conducted at a 5% confidence level. The algorithm was programmed to return whether the null hypothesis was rejected or not along with the p-value. The MATLAB script uses the variable "h", which produces "0" if accepted null hypothesis. If not, the algorithm indicates the null hypothesis was rejected by returning "1". The p-value in a t-test is the chance of finding a test statistic that is as severe as, or more extreme than, the observed value. Small p values cast doubt on the validity of the null hypothesis.

3. Results

To diagnose prostate cancer patients, the purpose of this study was to find any LBP-

based features that can classify benign and malignant tumours. The algorithm calculates four first-order and seven second-order statistics using True and False patient image data. A histogram feature provided first-order statistics, whereas GLRLM provided second-order statistics. Next, by carrying out a two-sample T-test, the aim was to confirm which of the statistics were better at classifying the patients as healthy and cancerous. Table 2 summarises the results obtained from the t-test for first-order statistics. The features mean and skewness gave a result of "0", indicating the acceptance of the null hypothesis. This result concludes no significant difference in the two populations at a 5% confidence interval. In contrast, the features SD and kurtosis produced a result of "1", indicating the rejection of the null hypothesis. This observed result concludes that these two features would better identify benign tumours from malignant tumours.

Table 2: Results of the two-sample t-test of the histogram features

Feature	**h**	**Accept/ Reject**	**p**
Mean	0	Accept	0.1898
SD	1	Reject	$7.5079e^{-04}$
Skewness	0	Accept	0.0794
Kurtosis	1	Reject	0.0300

Table 3 summarises the results of the two-sample t-test. The features SRE, LRE, GLN, RP, LGRE and HGRE gave a result of "0", indicating the acceptance of the null hypothesis. This result concludes no significant difference in the two populations at a 5% confidence interval. On the contrary, for the feature RLN, the result was "1", indicating the rejection of the null hypothesis. This observed result concludes that this feature would be better at identifying benign tumours from malignant tumours.

Table 3. Results of the two-sample t-test of the GLRLM features

Feature	**h**	**Accept / Reject**	**p**
SRE	0	Accept	0.4730
LRE	0	Accept	0.1099
GLN	0	Accept	0.0567
RP	0	Accept	0.0270
RLN	1	Reject	0.0207
LGRE	0	Accept	0.0614
HGRE	0	Accept	0.0578

4. Discussion

Texture characteristics from mpMRI images have previously been promoted as predictive biomarkers in prostate cancer. The suggested method generated first-order and second-order statistics to reveal LBP-based features to detect prostate tumours using mpMRI images. Eleven LBP texture features were assessed in the study. The researcher found three statistically significant ($P < 0.05$) features using a statistical evaluation approach. They were: first-order statistics SD (B-14.5611, M-16.5000), Kurtosis (B-54.5794, M-39.0421) and second-order statistic feature GLRLM-based RLN (B-5193.4605, M-4361.7848). The results obtained depict that the benign and malignant tumours can be distinguished using these three features. Future developments make it possible to improve algorithms for automatic detection of prostate cancer using the identified positive features. Assessed other features: Mean, Skewness, SRE, LRE, GLN, RP, LGRE and HGRE showed no statistical difference between the two categories. These negative results indicated that benign and malignant tumours could not be distinguished using these eight features.

GLRLM-based RLN has been effectively used in many cancer detection algorithms. A. Kunimatsu et al. (2018) used MRI image-based texture analysis to compare and elucidate

Primary Central Nervous System Lymphoma (PCNSL) and Glioblastoma (GBM) (Kunimatsu *et al.*, 2018). This research estimated first-order and second-order features using grey level co-occurrence matrix (GLCM), GLRLM, grey level size zone matrix, and multiple grey level size zone matrix. Out of all features computed, RP were the most effective texture characteristics for indicating differences between GBM and PCNSL. Unlike SD and kurtosis, this feature's unit of measurement has no physical explanation. As a result, more research needs to be conducted to support the use of this measure in clinical practice. The extraction of unique and robust textural primitives has a significant impact. If feature extraction does not lead to better texture representation, the intended results of the study shall not be attained. The demand for practical texture analysis and representation approaches grows, notably in medical image analysis, face recognition, biometrics, aerial imagery analysis, and content-based image retrieval. The LBP method was established by Ojala et al. The invariance of LBP to monotonic greyscale shift, modest computing complexity, and ease of implementation are its most notable features. For improved texture detection in ultrasound images of the liver, K. Aggarwal et al. (2016) used a modified LBP with the OTSU approach (Aggarwal, Bhamrah and Ryait, 2016). There were positive findings in identifying cirrhosis in the liver.

There are certain limitations to this research. Despite the fact that the chosen criteria resulted in an improved malignant patient diagnosis for the current dataset, malignant image misclassifications continue, which needs to be better understood. For patients with prostate cancer, tumour heterogeneity contributes as the main reason for mislabelling the images in the patient's image set. Although the patient's biopsy indicates that the tumour is malignant, and images reveal malignant characteristics, other images may have most or all benign features due to the tumour's possible heterogeneity. The second limitation of this study is having a limited dataset of benign and malignant prostate images, among which the number of benign images was greater than the number of malignant tumour images. In machine learning, small datasets can lead to the overfitting of models. As a result of an imbalanced dataset including fewer cancer image samples than benign image samples, the classifier will be biased toward the benign class and misclassify malignant labelled images. A possible suggestion to overcome this issue would be the synthetic minority oversampling technique. Another major limitation was the time constraint. With the lack of time, it was not possible to carry out the classification and validation process of the algorithm. Finally, a final constraint is the usage of 2D images rather than 3D images. For many of the same feature extraction methods employed in this work, other research comparing 2D and 3D MRI in cancer image analysis show that 3D imaging delivers higher classification performance than 2D pictures (Chen *et al.*, 2007; Arai, Herdiyeni and Okumura, 2012; Ortiz-Ramon *et al.*, 2017).

5. Conclusion

Pre-processing, ROI selection, feature extraction, and classification are the main stages that are usually followed in the medical image processing procedure. An approach for determining the optimum feature extraction method for categorising medical images is suggested in this study. This study aims to identify any histogram and GLRLM based features using LBP images and classify malignant and benign tumours of the prostate. Features were extracted from the LBP image using a histogram and the GLRLM operator for feature extraction. The study resulted in four histogram features and seven GLRLM features. Out of the eleven features, the study identified three positive features. Statistical testing confirmed a significant difference in the features between benign and malignant tumours. This research was conducted under limitations, such as imbalance and small image dataset, time constraint, and image misclassification.

Although the outcome of this prostate cancer detection method is positive, there is potential for development in the future. Due to time restrictions, it was impossible to carry out several other objectives to improve the research study. A real clinical analysis should be performed as the images were obtained from an open-access platform. The suggested algorithm's code could be enhanced and automated to categorise images by training classifiers. Along with improvement, the code needs to be cleaned up to improve performance. Future advancements might also involve using 3D volumetric images since 3D texture characteristics have been essential to better discrimination in machine learning systems. The proposed algorithm can also be compared with other image classification techniques such as LBP variants, GLCM and other techniques.

References

Aggarwal, K; Bhamrah, M S and Ryait, H S (2016): The identification of liver cirrhosis with modified LBP grayscaling and Otsu binarization, *SpringerPlus*, 5(1). Available at: https://doi.org/10.1186/s40064-016-1970-6.

Arai, K; Herdiyeni, Y and Okumura, H (2012): Comparison of 2D and 3D Local Binary Pattern in Lung Cancer Diagnosis, *International Journal of Advanced Computer Science and Applications*, 3(4). Available at: https://doi.org/10.14569/ijacsa.2012.030416.

Candefjord, S; Ramser, K and Lindahl, O A (2009): Technologies for localization and diagnosis of prostate cancer, *Journal of Medical Engineering and Technology*, 33(8), pp. 585–603. Available at: https://doi.org/10.3109/03091900903111966.

Catalona, W J and Loeb, S (2005): The PSA era is not over for prostate cancer, *European Urology*, 48(4), pp. 541–545. Available at: https://doi.org/10.1016/j.eururo.2005.07.014.

Chen, W; Giger, M L; Li, H; Bick, U and Newstead, G M (2007): Volumetric texture analysis of breast lesions on contrast-enhanced magnetic resonance images, *Magnetic Resonance in Medicine*, 58(3), pp. 562–571. Available at: https://doi.org/10.1002/mrm.21347.

Chu, A; Sehgal, CM and Greenleaf, J F (1990): Use of gray value distribution of run lengths for texture analysis, *Pattern Recognition Letters*, 11(6), pp. 415–419. Available at: https://doi.org/10.1016/0167-8655(90)90112-F.

Dinh, C V; Steenbergen, P; Ghobadi, G; Heijmink, S W T J P; Pos, F J; Haustermans, K and van der Heide, U A (2016): Magnetic resonance imaging for prostate cancer radiotherapy, *Physica Medica*, 32(3), pp. 446–451. Available at: https://doi.org/10.1016/j.ejmp.2016.01.484.

Elferink, W O (2021): *Gray Level Run Length Image Statistics*, *MATLAB Central File Exchnage*. Available at: https://www.mathworks.com/matlabcentral/fileexchange/52640-gray-level-run-length-image-statistics [Accessed: 8 November 2021].

Etzioni, R; Penson, D F; Legler, J M; di Tommaso, D; Boer, R; Gann, P H and Feuer, E J (2002): Overdiagnosis due to prostate-specific antigen screening: Lessons from U.S. prostate cancer incidence trends, *Journal of the National Cancer Institute*, 94(13), pp. 981–990. Available at: https://doi.org/10.1093/jnci/94.13.981.

Feng, J; Dong, Y; Liang, L and Pu, J (2015): Dominant – Completed Local Binary Pattern for Texture Classification, (August), pp. 233–238.

Fuchsjager, M; Shukla-Dave, A; Akin, O; Barentsz, J and Hriack, H (2008): Prostate cancer imaging, *Acta Radiologica*, 49(1), pp. 107–120. Available at: https://doi.org/10.1080/02841850701545821.

Galloway, M M (1975): Texture analysis using gray level run lengths, *Computer Graphics and*

Image Processing, 4(2), pp. 172–179. Available at: https://doi.org/10.1016/s0146-664x(75)80008-6.

Litjens, G; Debats, O; Barentsz, J; Karssemeijer, N and Huisman, H (2017): *ProstateX Challenge data*, *The Cancer Imaging Archive*. Available at: https://doi.org/https://doi.org/10.7937/K9TCIA.2017.MURS5CL.

Haralick, R M; Dinstein, I and Shanmugam, K (1973): Textural Features for Image Classification, *IEEE Transactions on Systems, Man and Cybernetics*, SMC-3(6), pp. 610–621. Available at: https://doi.org/10.1109/TSMC.1973.4309314.

Hricak, H; Choyke, P L; Eberhardt, S C; Leibel, S A and Scardino, P T (2007): Imaging prostate cancer: A multidisciplinary perspective, *Radiology*, 243(1), pp. 28–53. Available at: https://doi.org/10.1148/radiol.2431030580.

Clark, K; Vendt, B; Smith, K; Freymann, J; Kirby, J; Koppel, P; Moore, S; Phillips, S; Maffitt, D; Pringle, M; Tarbox, L and Prior, F (2013): The Cancer Imaging Archive (TCIA): Maintaining and Operating a Public Information Repository, *Journal of Digital Imaging*, 26(6), pp. 1045–1057. Available at: https://doi.org/https://doi.org/10.1007/s10278-013-9622-7.

Kunimatsu, A; Kunimatsu, N; Kamiya, K; Watadani, T; Mori, H and Abe, O (2018): Comparison between glioblastoma and primary central nervous system lymphoma using MR image-based texture analysis, *Magnetic Resonance in Medical Sciences*, 17(1), pp. 50–57. Available at: https://doi.org/10.2463/mrms.mp.2017-0044.

Litjens, G; Debats, O; Barentsz, J; Karssemeijer, N and Huisman, H (2014): Computer-aided detection of prostate cancer in MRI, *IEEE Transactions on Medical Imaging*, 33(5), pp. 1083–1092. Available at: https://doi.org/10.1109/TMI.2014.2303821.

Mitchell, R E; Shah, J B; Desai, M; Goluboff, E T; Katz, A E; Petrylak, D P; Olsson, C A; Benson, M C and McKiernan, J M (2005): 948: Has Pre-Operative PSA Lost the Ability to Predict Biochemical Failure after Radical Retropubic Prostatectomy?, *Journal of Urology*, 173(4S), pp. 256–257. Available at: https://doi.org/10.1016/s0022-5347(18)35104-8.

Ojala, T; Valkealahti, K; Oja, E and Pietikäinen, M (2001): Texture discrimination with multidimensional distributions of signed gray-level differences, *Pattern Recognition*, 34(3), pp. 727–739. Available at: https://doi.org/https://doi.org/10.1016/S0031-3203(00)00010-8.

Ojala, T, Pietikäinen, M and Harwood, D (1996): A comparative study of texture measures with classification based on featured distributions, *Pattern Recognition*, 29(1), pp. 51–59. Available at: https://doi.org/https://doi.org/10.1016/0031-3203(95)00067-4.

Ortiz-Ramon, R; Larroza, A; Arana, E and Moratal, D (2017): 'A radiomics evaluation of 2D and 3D MRI texture features to classify brain metastases from lung cancer and melanoma', *Proceedings of the Annual International Conference of the IEEE Engineering in Medicine and Biology Society, EMBS*. Institute of Electrical and Electronics Engineers Inc., pp. 493–496. Available at: https://doi.org/10.1109/EMBC.2017.8036869.

Schröder, F H and Roobol, M J (2009): Defining the optimal prostate-specific antigen threshold for the diagnosis of prostate cancer, *Current Opinion in Urology*, 19(3), pp. 227–231. Available at: https://doi.org/10.1097/MOU.0b013e328329a2d0.

Seitz, M; Osman, M and Choyke, P L (2009): Functional Magnetic Resonance Imaging in Prostate Cancer, *European Urology*, 55(4), pp. 801–814. Available at: https://doi.org/10.1016/j.eururo.2009.01.027.

Turkbey, B; Brown, A M; Sankineni, S; Wood, B J; Pinto, P A and Choyke, P L (2016): Multiparametric prostate magnetic resonance imaging in the evaluation of prostate cancer, *CA: A Cancer Journal for Clinicians*, 66(4), pp. 326–336. Available at: https://doi.org/10.3322/caac.21333.

Weinreb, J C; Blume, J D; Coakley, F V; Wheeler, T M; Cormack, J B.; Sotto, C K; Cho, H; Kawashima, A; Tempany-Afdhal, C M; Macura, K J.; Rosen, M; Gerst, S R and Kurhanewicz, J (2009): Prostate cancer: Sextant localization at MR imaging and MR spectroscopic imaging before prostatectomy - Results of ACRIN prospective multi-institutional clinicopathologic study, *Radiology*, 251(1), pp. 122–133. Available at: https://doi.org/10.1148/radiol.2511080409.

Acknowladgment

First and foremost, I want to express my gratitude to my supervisor, Mr EHADK Hewadikaram, and co-supervisor, Mr RMUKGMS Bandara, for their assistance throughout this research. Next, I owe a huge debt of gratitude to Mr WLPK Wijesinghe, lecturer at Department of Electrical, Electronic and Telecommunication, General Sir John Kotelawela Defence University, for giving me really helpful comments and supporting me to correct myself during this research. I would also like to thank the Cancer Imaging Archive (TCIA) for making the PROSTATEx Challenge image collection available to the public. I thank Global Cancer Observatory and IARC Publications for making the global statistics available for research work.

Author Biography

KAI Harsha holds a BSc (Hons) in Biomedical Engineering from General Sir John Kotelawala Defence University, expecting to graduate in the Year 2022. Currently, she is following a MSc in Biomedical Engineering from General Sir John Kotelawala Defence University.

Dr.Rathnayaka received his B.Sc. in physical science, M.Sc. in Medical Physics, and Ph.D. in Bio-Medical Imaging Physics, from the University of Colombo, Sri Lanka. Currently he is a Post-Doctoral Fellow at Utsouthwestern, University of Texas, USA.

Mr. EHADK Hewadikaram is a senior lecturer in physics, Department of Electrical, Electronics and Telecommunication Engineering at General Sir John Kotelawala Defence university. After his graduation from University of Colombo, he completed an MSc in physics at Central Michigan University, USA and MPhil (Medical Physics), University of Colombo. His research interests are ultrasound, nuclear medicine, radiation protection and medical imaging.